2

ARMY RESEARCH LABORATORY

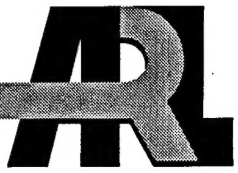

Wideband Pulse Attenuation of an Uncured Metallized Glass Fiber Mat

by William O. Coburn and Christian G. Reiff

ARL-TR-790

September 1995

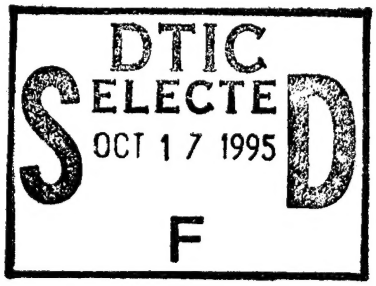

The findings in this report are not to be construed as an official Department of the Army position unless so designated by other authorized documents.

Citation of manufacturer's or trade names does not constitute an official endorsement or approval of the use thereof.

Destroy this report when it is no longer needed. Do not return it to the originator.

REPORT DOCUMENTATION PAGE

Form Approved
OMB No. 0704-0188

1. AGENCY USE ONLY *(Leave blank)*	2. REPORT DATE	3. REPORT TYPE AND DATES COVERED
	September 1995	Final, 1 Dec 1994 to 20 Jan 1995

4. TITLE AND SUBTITLE
Wideband Pulse Attenuation of an Uncured Metallized Glass Fiber Mat

5. FUNDING NUMBERS
PE: 62120

6. AUTHOR(S)
William O. Coburn and Christian G. Reiff

7. PERFORMING ORGANIZATION NAME(S) AND ADDRESS(ES)
U.S. Army Research Laboratory
Attn: AMSRL-WT-ND
2800 Powder Mill Road
Adelphi, MD 20783-1197

8. PERFORMING ORGANIZATION REPORT NUMBER
ARL-TR-790

9. SPONSORING/MONITORING AGENCY NAME(S) AND ADDRESS(ES)
U.S. Army Research Laboratory
2800 Powder Mill Road
Adelphi, MD 20783-1197

10. SPONSORING/MONITORING AGENCY REPORT NUMBER

11. SUPPLEMENTARY NOTES
AMS code: 622120.H25001
ARL PR: 5FE7E5

12a. DISTRIBUTION/AVAILABILITY STATEMENT
Approved for public release; distribution unlimited.

12b. DISTRIBUTION CODE

13. ABSTRACT *(Maximum 200 words)*

Metallized glass fiber (MGF) is a glass fiber substrate with a metal coating that can be used to improve the electrical properties of reinforced composites. The material considered here (RoMHOglas™ Metallized Glass Conductive Fibers, produced by Lundy Technical Center, Pompano Beach, FL) is an E-glass fiber metallized with aluminum and processed into a nonwoven mat. The U.S. Army Research Laboratory (ARL) is interested in evaluating such materials as an alternative to metals for electromagnetic shielding. In this preliminary study, the MGF mat was left uncured so that the basic properties of RoMHOglas™ could be investigated before the material was incorporated into a reinforced composite material. The ARL Scale Model Facility was used to characterize the shielding effectiveness (SE) of a planar sample of RoMHOglas™ by measurements of the wideband pulse attenuation of the material. The experimental technique and its application for SE measurements are discussed. The attenuation of the pulse peak amplitude is 39 dB, and the corresponding frequency-dependent SE provides a reference for the electromagnetic properties of this commercially available composite material.

14. SUBJECT TERMS
Metallized glass fiber, fast-pulse penetration, shielding effectiveness, RoMHOglas™

15. NUMBER OF PAGES
23

16. PRICE CODE

17. SECURITY CLASSIFICATION OF REPORT	18. SECURITY CLASSIFICATION OF THIS PAGE	19. SECURITY CLASSIFICATION OF ABSTRACT	20. LIMITATION OF ABSTRACT
Unclassified	Unclassified	Unclassified	UL

NSN 7540-01-280-5500

Standard Form 298 (Rev. 2-89)
Prescribed by ANSI Std. Z39-18
298-102

Contents

Figures

Tables

1. Introduction

Metallized glass fiber (MGF) is a glass fiber substrate with a metal coating that is manufactured as a multifilament continuous strand. MGF can be processed into typical fiberglass reinforcement configurations and used to modify the properties of polymeric composites [1]. MGF can be incorporated to improve the thermal and electrical conductivity of reinforced composites, and an optimum design can retain the desired physical properties [1,2]. The U.S. Army Research Laboratory (ARL) is interested in evaluating such materials as an alternative to metals for electromagnetic (EM) shielding [3]. MGF in a random-orientation mat could provide good electrical properties that are roughly isotropic at frequencies below a few hundred megahertz.

The material considered here (product name RoMHOglas™) is an E-glass fiber (average diameter 0.7 mils) metallized with aluminum. RoMHOglas™ is available from Lundy Technical Center, Pompano Beach, FL, in 36-in. wide rolls of MGF nonwoven mat (½ or ¼ oz/ft^2). In this preliminary study, the MGF mat was left uncured so that we could investigate the basic properties of this material before it was incorporated into a reinforced composite. The thickness of the nonwoven mat is nonuniform but is estimated to be 1/16 in. in the relatively compressed state when taken off the roll. The metallized layer is a continuous Al film bonded to the glass fiber with 50- to 100-percent coverage. The average dc resistance of the monofilament MGF is 2.5 ohm/cm, and by weight the mat is 37-percent glass and 63-percent Al [1].

Assuming a uniform Al coating on an 18-μm-diameter substrate and a conductivity, σ_{Al}, of 2.9×10^7 mho/m, the above dc resistance implies a metal thickness $d \approx 1/4$ μm. The EM absorption in the Al layer depends on the skin depth, $\delta_{Al} = 1/\sqrt{\pi\mu\sigma_{Al}f}$, where μ is the permeability and f is frequency. The absorption in one Al layer is small (compared to the surface reflection) because δ_{Al} is much greater than δ for the frequencies of interest. When formed into a mat, the MGFs lead to an effective sample conductivity, σ_{eff}, which is the parameter of interest for EM reflection. For cured samples, this σ_{eff} increases exponentially with the fibers loading density and is about 400 mho/m (based on the measured R_{dc}) for 50-percent loading of 0.5-in. chopped strand [1]. We prefer to determine σ_{eff} from the measured SE, under conditions for which the exact solution is available, as R_{dc} measurements can be complicated by poor electrical contact to the sample. Previous results for the EM characterization of RoMHOglas™ ($f < 100$ MHz) indicate that for cured samples, of MGF mat (i.e., high loading densities), $\sigma_{eff} \approx 2000$ mho/m [4]. However, uncured samples exhibit practically no EM reflection at these frequencies, which implies an extremely low σ_{eff}.

We used the ARL Scale Model Facility (SMF) to investigate the shielding effectiveness (SE) of the uncured MGF mat for $f > 100$ MHz, by measuring the "fast" (i.e., wideband) pulse attenuation of a planar sample. The

fore spurious reflections or edge diffractions are observed. In this manner, the SE of the sample can be characterized in the frequency range from 100 to 2000 MHz. The measured SE for the uncured MGF mat provides a reference for the EM properties of this commercially available composite material. We will similarly test samples cured in various ways to identify the approach that maximizes σ_{eff}.

2. Experiment

The ARL SMF can radiate a repetitive, horizontally polarized electric (*E*-) field pulse with a nominal risetime ≈ 0.2 ns and pulse width ≈ 1 ns. Time-domain sampling techniques allow signal averaging of sensor responses, which greatly enhances the signal-to-noise ratio (SNR) of the measured transients. More detailed descriptions of the SMF pulser and data acquisition instrumentation are available elsewhere [5–9]. EM sensors, calibration techniques, and data compensation algorithms have been developed for accurate recording of picosecond regime events [6].

The instrumentation for these experiments is listed in table 1. The field sensor used is an asymptotic monopole that responds to the time derivative of the electric displacement field (D-dot). The test setup is shown in figure 1, which indicates the physical relationship between the source dipole antenna (shown in fig. 2) and the D-dot sensor.

A 106 × 106-in. planar sample was constructed from three strips (36 in. wide) of ¼ oz/ft^2 RoMHOglas™, overlapped by at least 1 in. in two places, and taped together with nonconductive tape. Electrical contact between the sheets of MGF nonwoven mat was maintained only by the pressure provided by tape on each side of the sample. This approach was designed to model the layup of MGF mat where no special provisions are made for overlapping laminates. This RoMHOglas™ sample is placed between the source dipole and D-dot sensor, which are at a height of 3.7 m above ground, as shown in figure 3. Polarization effects were not investigated, and the results correspond to an incident *E*-field oriented across the strips of MGF (i.e., across the vertical seams). This corresponds to the worst-case polarization for seam leakage that would be resonant for frequencies above 50 MHz.

The experimental objective was to measure the horizontally polarized *E*-field pulse with and without the MGF barrier placed between the source dipole and D-dot sensor. The barrier was suspended so that it could be removed without disturbance to the physical positioning of the measurement sensor relative to the radiation source. The dimensions of the source antenna, the MGF barrier, and the experimental arrangement are such that

Table 1. Instrumentation for pulse penetration experiments.

Instrumentation	Description
D-dot sensor	ARL asymptotic monopole (model D-4)
Rf cables	Andrews heliax cable
Pulse generator	ARL pulse generator (1 kV into 50 Ω, with 154-ps rise-time and 1-ns pulse width)
Antenna	ARL SMF dipole antenna
Data acquisition	Tektronix 7854 sampling oscilloscope Tektronix 7S12 time-domain sampler Tektronix S-6 sampling head Tektronix S-53 trigger recognizer
Data processing	386 PC and MATLAB™

Figure 1. Physical relationship between dipole antenna and sensor (drawn to scale).

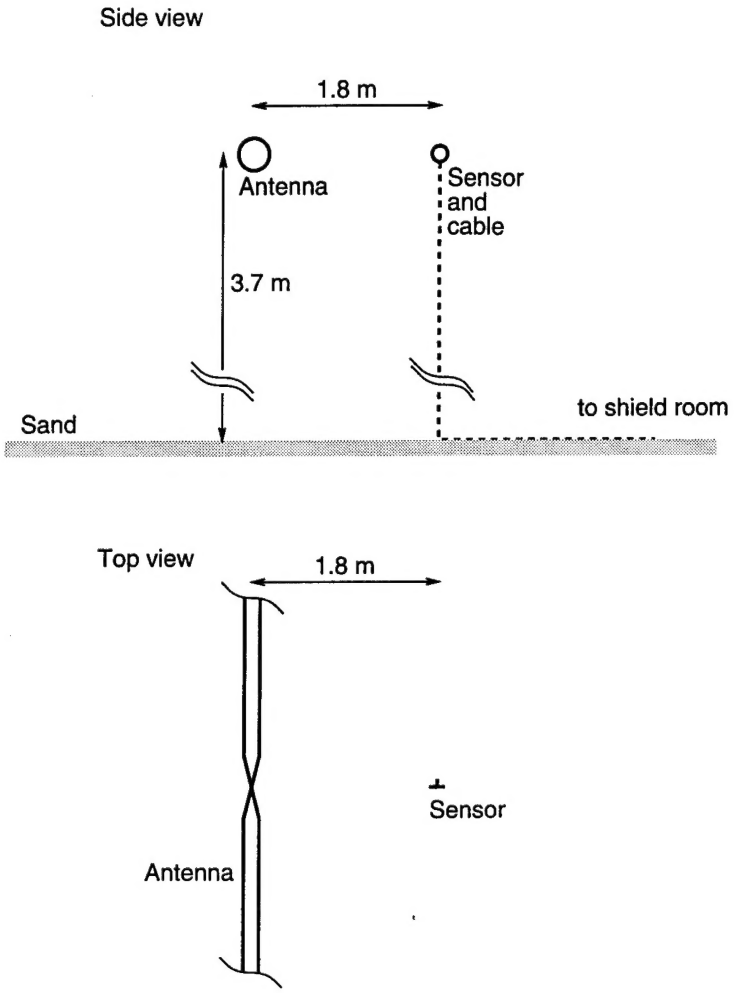

Figure 2. Scale model facility (SMF) dipole antenna.

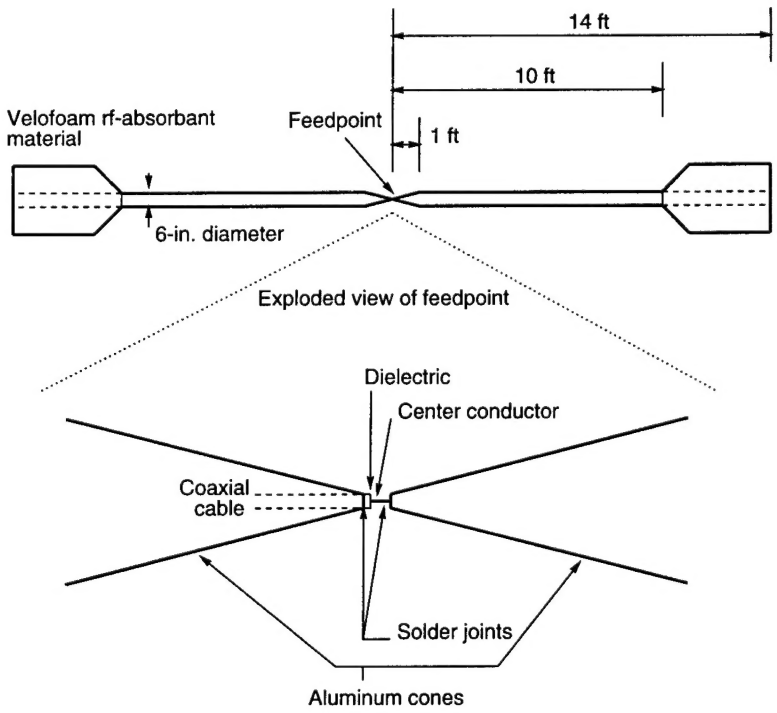

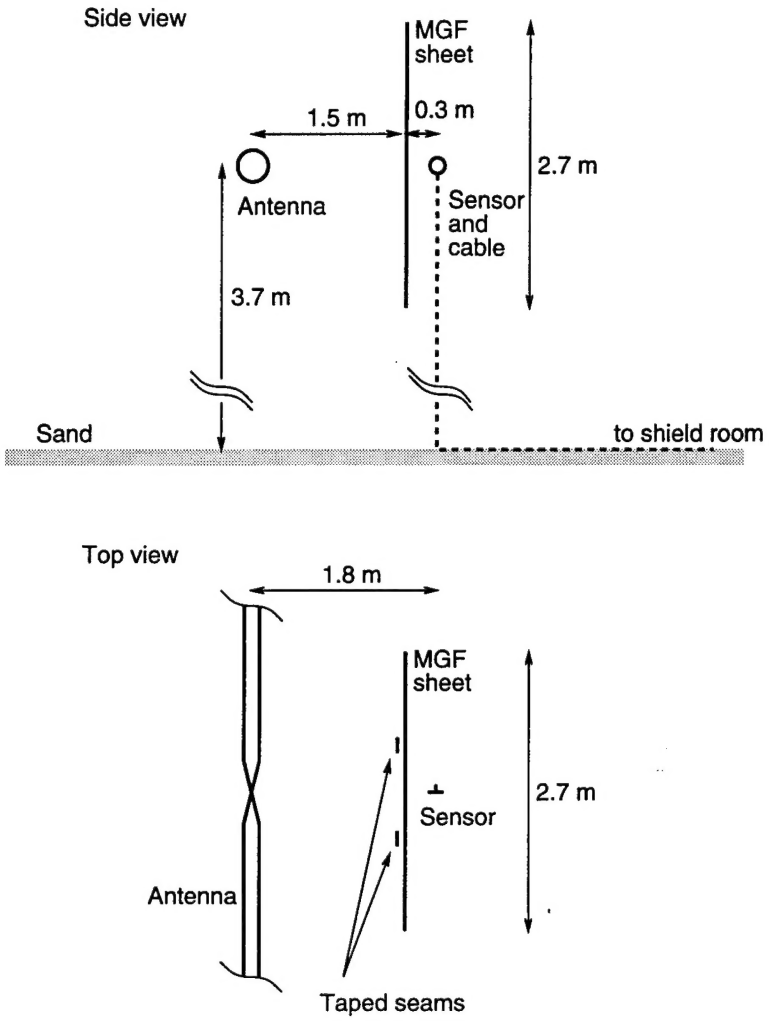

Figure 3. Physical relationship between dipole, MGF sheet, and sensor (drawn to scale).

a nominal 4-ns "clear-time" window is obtained at the measurement location. In this manner the incident (or attenuated) pulse can be recorded before complicating effects such as reflections are observed. The MGF sample is sufficiently large that the attenuated pulse can be recorded before the effects of edge diffraction are observed at the sensor location. These attenuation measurements can be used to determine SE, but since the incident pulse may not be a true plane wave, the results may not be completely equivalent to plane-wave SE.

2.1 Plane Wave Approximation

In these SE experiments, the sample must be sufficiently close to the SMF source antenna that we obtain an adequate SNR for the attenuated measurement. For this reason the sample is located so that the field incident on the MGF mat (fig. 3) only approximates a plane wave. For a source of maximum dimension, D, the far field conditions are [10]

$$r > 2D^2/\lambda \ , \tag{1}$$

$$r >> D, \text{ and} \tag{2}$$

$$r >> \lambda \ , \tag{3}$$

where r is the observation point (1.5 m) and λ is the wavelength. If the observer is located at a point that satisfies all these relations, then far-field radiation and plane-wave conditions would be obtained. If equations (1) to (3) are satisfied over the entire sample, then the incident field can be assumed to be a plane wave, which allows simplification in the EM analysis of SMF experiments.

Because of the impulsive nature of the SMF source, the radiating section of the antenna is that which is "seen" during a given time. For the SMF source antenna, D is twice the length of the biconic feed section over which the pulse could propagate during the time of interest. Based on the sampling theorem in information transmission [11], we associate early times with high frequencies according to $t \approx 1/2f$. So for propagation at the speed of light, $c = 3 \times 10^8$ m/s, we estimate the maximum antenna dimension in terms of frequency as

$$D \approx 2ct \approx \frac{2c}{2f} = \lambda \ . \tag{4}$$

Then equation (1) implies that $r > 2\lambda$, while equation (2) implies that $r >> \lambda$. In these experiments, equation (1) is satisfied above 400 MHz, but equation (2) is only weakly satisfied in the range from 400 to 2000 MHz. Conditions (1) and (2) are required for the amplitude approximation to the far fields [10], but since (2) is only weakly satisfied, the incident wavefront is not planar. Condition (3) is weakly satisfied in the frequency range from 400 to 2000 MHz, and all three conditions would be fully satisfied above 2000 MHz. Thus we consider the plane-wave approximation to be reasonable for frequencies above about 400 MHz.

Since the SMF source antenna does not produce a plane wave over the entire MGF sample at all frequencies, the measured attenuation may not be directly related to plane-wave SE. For a spherical wave, decaying inversely with distance from the SMF antenna feedpoint, the incident-field amplitude at the edge of the MGF barrier would be 41 percent less than at the center. An average of incident-field measurements could be about 20 percent less than the incident field measured under uniform illumination, and the measured attenuation would be 1.6 dB less than for plane-wave SE. The phase difference from the sample center to edge at 2000 MHz is 11° or 59 percent. Although these variations over the MGF sample may not be negligible, they do not introduce large errors when the SMF is used to approximate plane-wave SE measurements.

The incident-wave impedance is also important for SE measurements since it determines the surface reflection. For an arbitrary source, the wave impedance of the radiated field, Z_w, approaches that of free space, $Z_0 = 120\pi$

ohms, when r becomes large compared to wavelength. The wave impedance of a high-impedance (E-field) source, such as the SMF dipole antenna, is

$$Z_w = Z_0 \frac{\lambda}{2\pi r} \text{ for } r \leq \frac{\lambda}{2\pi}, \text{ and} \tag{5}$$

$$Z_w = Z_0 \text{ for } r \geq \frac{\lambda}{2\pi}, \tag{6}$$

provided that $D << \lambda$ [12]. In these experiments $Z_w \approx Z_0$ at frequencies above 32 MHz, but $D \approx \lambda$, so that the incident field only approximates a plane wave. Small discrepancies in the incident-wave impedance compared to Z_0 would not lead to large errors in the correlation of these attenuation measurements to plane-wave SE. Correction factors based on the measured Z_w could be used for removing this source of error in the correlation to plane-wave SE. The results for the uncured MGF sample imply that the dominant loss mechanism is EM absorption. In this case the plane-wave approximation is required only if we assume uniform illumination in the theoretical analysis of the experimental configuration.

Although the SMF antenna is not electrically small in the usual sense, SE measurements using the SMF should still be representative of plane-wave SE. The wave impedance of the radiated field should be measured and used to correct the SMF SE data for any difference in surface reflection due to the incident-wave impedance. For large samples, the spherical nature of the incident wavefront should be taken into account. The incident and attenuated fields could be sampled across the barrier, and an average, weighted according to position, used to calculate SE. These techniques will be used in the future so that fast-pulse attenuation measurements can better correspond to plane-wave SE when conditions (1) to (3) and those required for the validity of equation (6) are only weakly satisfied. The combined experimental error for the SMF SE measurement is estimated independently of the correlation of these data to plane-wave SE.

2.2 Experimental Error

The experiment was simplified by our use of the substitution method for quantifying the attenuation of the MGF barrier. The radiation source dipole antenna and D-dot sensor remained at fixed positions so that physical positioning errors are minimized for comparative measurements. The D-dot sensor transient response is recorded with and without the MGF barrier. The measured data are numerically integrated, converted to E-field magnitudes, and transformed into the frequency domain. The difference (in decibels) between the frequency spectrum magnitudes (of the D-dot or E-field data) represents the measured SE. There is a random error involved, as some changes in the field strength and/or measurement system can occur between the incident and attenuated field measurements. Although the typical transient measurement repeatability is ±5 percent [9], the repeatability for small-signal measurements depends on the number of signal averages used in the data acquisition and can result in a ±10-percent

error [13]. We take the measurement repeatability for the incident pulse to be ±5 percent, but for the attenuated pulse we use a repeatability error of ±10 percent.

Sources of error from the physical placement and orientation of the D-dot sensor are typically ±5 percent, but in the substitution method for SE these errors are minimized, as the experimental configuration is unchanged between measurements. To bound the total error associated with the measured data, we assign a random experimental error of ±10 percent due to undetected aspects such as measurement system gain fluctuations, variations in the EM environment, data processing errors, etc. The total experimental error is the combination of these sources of error, which are assumed to be random and independent. So the total error associated with the incident pulse data is $\sqrt{(0.05)^2 + (0.1)^2} = \pm 11$ percent, while that associated with the attenuated pulse data is $\sqrt{(0.1)^2 + (0.1)^2} = \pm 14$ percent. Then the measured SE, which is the ratio of measurements made before and after the MGF mat is installed (with an uncertainty of ±11 and ±14 percent, respectively), has an estimated total error of ±18 percent (1.4 dB) when the fast-pulse attenuation technique is used.

3. Results

The transient results are shown in figure 4, before and after insertion of the uncured RoMHOglas™ barrier. The peak radiated *E*-field at the sensor location is 197 V/m and has a high SNR, as shown in figure 4(a). The received pulse measured in the presence of the MGF sample has a peak amplitude of 2.25 V/m, as shown in figure 4(b). The leading edge of this transient is an artifact of the numerical integration of the D-dot sensor output. The lower SNR of the attenuated data leads to a higher error bound, which can be reduced in future measurements by a moderate increase in incident-field level or by low-noise amplification at the sensor output. The D-dot sensor peak output without the MGF barrier and the minimum noise level with the barrier imply a typical measurement dynamic range of 62 dB for these attenuation measurements. The results for this uncured ¼ oz/ft^2 RoMHOglas™ sample indicate a time-domain SE of about 39 dB for the peak of the SMF *E*-field pulse.

The results in the Fourier transform space are shown in figure 5. The useful frequency content of the incident pulse should be bounded to approximately 100 to 3000 MHz (fig. 5(a)). The reduced amplitude and frequency content of the measurement made after the MGF mat is installed are due to the SE of the sample. The small-signal measurements required in this experiment have a poor SNR beyond 2000 MHz, as can be inferred from figure 5(b). This leads to an ambiguous result for quantifying SE measurements above 2000 MHz. These attenuation measurements provide useful SE data in the range from 100 to 2000 MHz, but based on the plane-wave approximation, the use of this technique to estimate plane-wave reflection is limited to frequencies above 400 MHz.

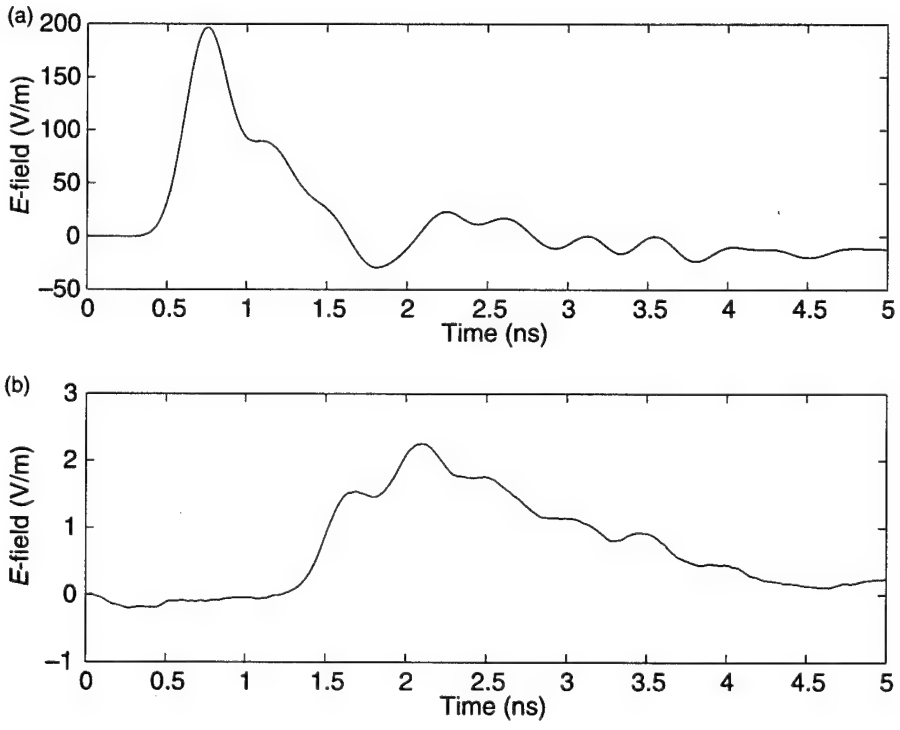

Figure 4. Electric field measurements (a) without barrier and (b) with barrier. Times zero of transients are not related.

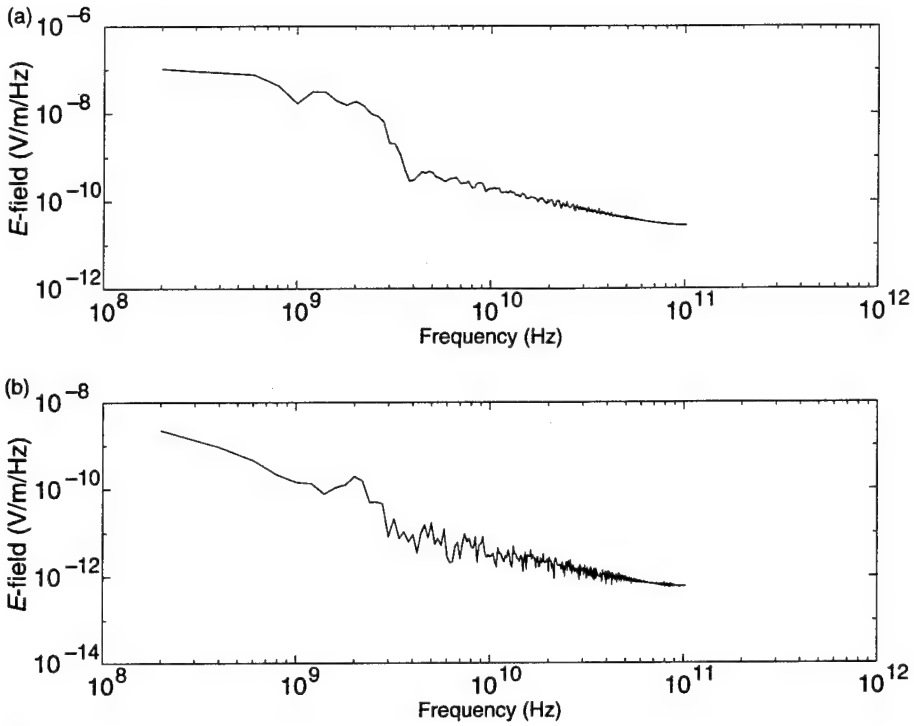

Figure 5. Electric field magnitude in Fourier transform space (a) without barrier and (b) with barrier.

The ratio (in decibels) of the measurements made before and after insertion of the MGF mat is plotted as a function of frequency in figure 6. The ratio was obtained with routines that filter the data [14,15] above 3000 MHz, where the incident pulse spectral content is negligible. This allows the SE ratio to be calculated without problems caused by the high-frequency portion of the spectrum, which has a poor SNR. This transfer function (100 to 2000 MHz) represents the sample SE as measured with the fast-pulse attenuation technique, where the amplitude and phase variations of the incident field over the MGF sample are neglected. The results can be interpreted as the plane-wave SE in the range from 400 to 2000 MHz with an uncertainty, compared to a truly planar incident field over the entire sample, of the same order as the total experimental error in determining SE (1.6 dB).

Although some error is involved in interpreting the SMF SE data as plane-wave SE, the results (fig. 6) demonstrate the expected trend for plane-wave illumination, in that the SE is roughly constant until absorption begins to dominate [12]. According to figure 6, absorption begins to become important above 200 MHz. This result indicates the increased attenuation associated with EM absorption in good conductors, namely the metallized Al layers. The high-frequency variations are believed to be associated with the nonuniform (and possibly anisotropic) nature of the MGF mat.

SE data for RoMHOglas™ are shown in figure 7 from 100 to 1000 MHz (reproduced from Warfel [1]) for a 50-percent loading density, ⅛-in.-thick, cured sample. These data are characteristic of *E*-field SE in that they decrease at 20 dB per decade increase in frequency until plane-wave conditions are obtained [12]. Since Warfel does not provide the details of the test technique [1], the relationship of these measured data to plane-wave SE

Figure 6. Shielding effectiveness of MGF sheet versus frequency.

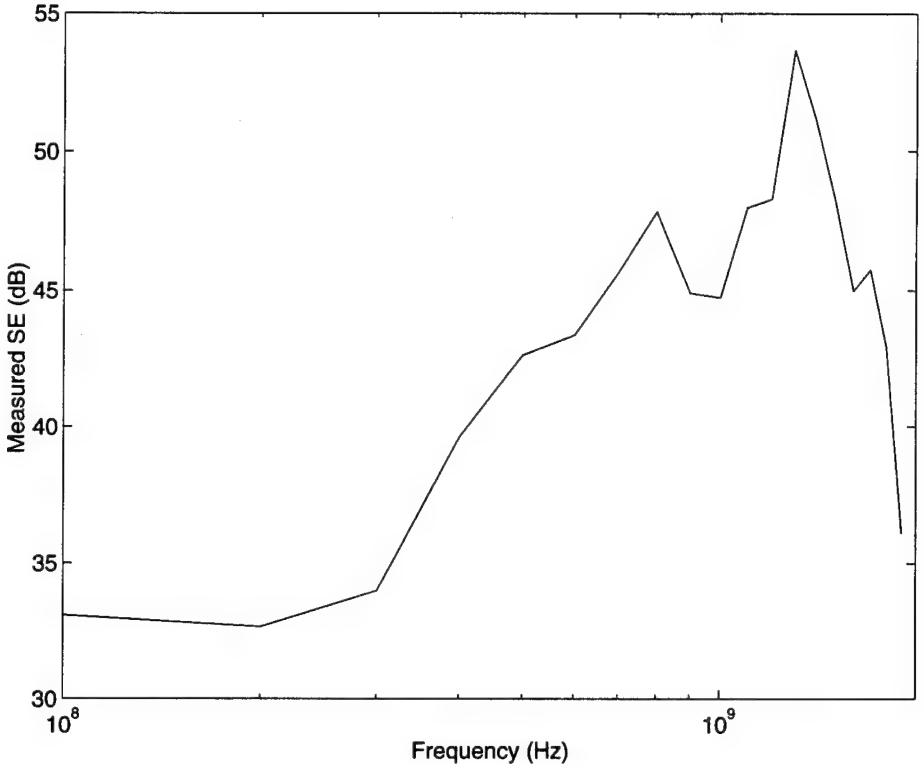

Figure 7. SE data for 0.5-in. chopped-strand MGF, 50-percent loading density, ⅛-in. thick cured sample.

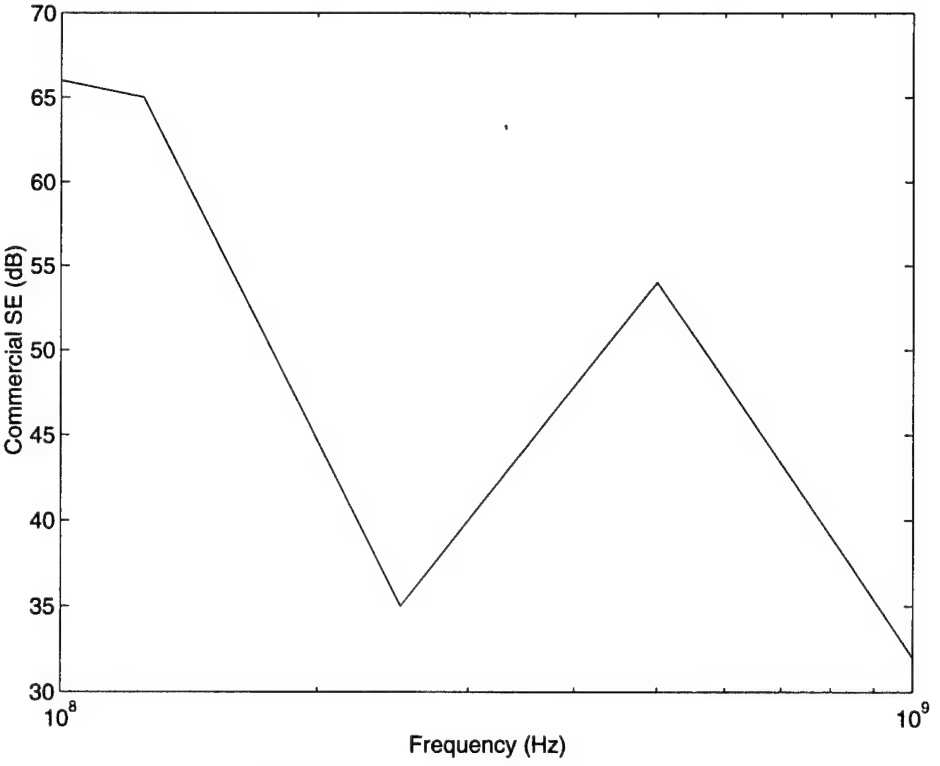

cannot be confirmed. However, if we assume $\sigma_{eff} \approx 400$ mho/m for these cured samples, the plane-wave SE (neglecting multiple reflections) at 200 MHz would be about 50 dB [12], which is consistent with figure 7. For uncured samples, the nature of the nonwoven mat implies a nonuniform and very low surface resistance owing to the poor electrical contact among the MGFs.

The σ_{eff} concept is not really appropriate for uncured MGF, and an uncured sample provides very little EM reflection. One possible model for the SE of an uncured mat is an extremely low σ_{eff}, combined with some EM absorption in the metallized Al. The calculated reflection, R, is shown in table 2 versus frequency for $\sigma_{eff} = 10$ and 100 mho/m. The 1/16-in.-thick nonwoven mat could contain at most 90 fibers oriented perpendicular to and stacked across the sample thickness. For uncured samples, the MGFs are not in close contact, and 45 fibers across the sample thickness would probably be a better estimate. In the limiting case of 50-percent Al coverage on each fiber, we would have 45 Al layers, whereas for 100-percent coverage we would have 90 Al layers. Included in table 2 is the calculated absorption, A, for an EM wave passing through 45 and 90 Al layers of individual thickness 0.24 μm. The nonwoven MGF mat actually has a random and twisted fiber orientation, so that A could be highly nonuniform over the sample. We consider an Al thickness of 10.8 μm to characterize A, and a low σ_{eff} to characterize R. For comparison to the measured SE, A for 10.8 μm of Al and R for $\sigma_{eff} = 10$ or 100 mho/m are combined to form the total SE, neglecting multiple reflections (table 2).

The combination of A and R (for $\sigma_{eff} = 10$ or 100 mho/m) is shown in figure 8 in comparison to the measured SE (fig. 6). Similar trends are evident, and the comparison demonstrates that EM absorption, even for a very thin Al coating thickness, dominates the SE of the uncured MGF mat. For cured samples, the σ_{eff} implied from the SE data and R_{dc} measurements of Warfel [1] is consistent with that determined by Latess et al [4] but is highly dependent on the details of the sample construction (i.e., fiber length, loading density, etc) and the curing process. The SMF SE measurements imply that the uncured MGF can have an extremely low σ_{eff}, so A would be the only significant mechanism for SE.

The MGF barrier had two seams (≈3 m long), and some seam leakage above 50 MHz might be expected to reduce the attenuation. At higher frequencies, this seam leakage would dominate the measured SE. Since this is not apparent, the results imply that the overlapped seams provide an electrical continuity at least as good as the uncured MGF mat. We believe the drop in SE above 1000 MHz to be typical of mesh materials. In particular, for metallized textile materials, the SE can be complicated, especially for a surface resistivity greater than 30 mΩ per square [16]. The reduced SE at high frequency typical of a simple mesh depends on the mesh spacing, g

Table 2. Calculated absorption, reflection, and combined attenuation.

	Calculated absorption, A (dB)		Calculated reflection, R (dB)		Total SE for 45 Al layers (dB)	
Frequency (MHz)	45 layers, d = 10.8 μm	90 layers, d = 21.6 μm	σ_{eff} = 10 mho/m	σ_{eff} = 100 mho/m	σ_{eff} = 10 mho/m	σ_{eff} = 100 mho/m
100	10	20	21	31	31	41
300	18	35	16	26	33	43
500	23	45	14	24	36	46
1000	32	63	11	21	43	53
2000	45	89	8	18	53	63

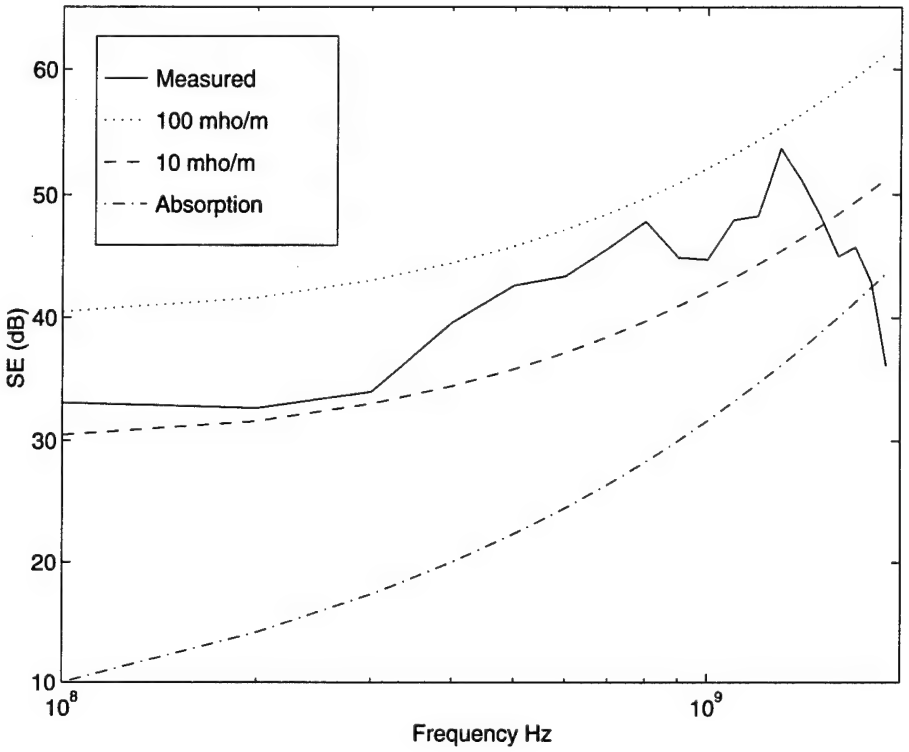

Figure 8. Calculated absorption and absorption combined with reflection in comparison to measured SE.

(in inches), compared to wavelength. The attenuation associated with the openness of the material decreases with frequency, f_{MHz} (in megahertz), according to [12]

$$\text{SE of mesh} = 20 \log\left(\frac{5906}{g f_{\mathrm{MHz}}}\right) \text{dB} \ . \tag{7}$$

Thus when the SE of mesh drops below the material SE, the measured attenuation will begin to decrease at 20 dB per decade increase in frequency. The measured SE (fig. 6) drops near 1000 MHz, which implies a seemingly large mesh spacing. Based on equation (7), $g \approx 10$ mils would reduce the measured SE to below 55 dB at 1000 MHz. Similar results were found by Fairneny [16] for metallized materials with a high surface resistivity, in that an equivalent thickness model based on the metal areal density showed poor agreement only for these types of materials. Using this model and a thickness of 10.8 μm for the uncured MGF SE would imply an areal density an order of magnitude less than that of typical metallized textiles [16]. For MGF nonwoven mat, the mesh spacing is nonuniform, and gaps much larger than the fiber diameter are not unreasonable. The measured results indicate that the composite structure and electrical properties of cured and uncured MGF samples are drastically different.

4. Conclusions

The versatility and excellent electrical properties of MGF make it an attractive material for EM shielding concepts. Even in an uncured sample, the electrical continuity of the MGF mat is sufficient to provide some SE, but the uncured material exhibits a much lower σ_{eff} than does a cured sample. This is as expected, since fiber-reinforced composites are typically cured under pressure, which would provide closer contact among the fibers. The nonconductive Al oxide layer associated with the coated fibers does not appear to prevent electrical continuity in cured samples, as the fibers are in close contact. However, the nature of the uncured mat implies that the fibers are not in close contact, and the sample would exhibit a low σ_{eff} and a correspondingly high surface resistivity.

Seam leakage would have been seen in the attenuated transient (depending on the SNR) but there was not an obvious degradation, because seams were present. This result implies that the electrical continuity provided by the overlapped seams is at least as good as the sample surface resistivity. The obvious conclusion is that the uncured MGF sample has an extremely low σ_{eff} and that A in the Al coating is the dominant mechanism for SE in uncured samples. This absorption should be retained in cured samples, while σ_{eff} would be larger but depend on the details of the sample construction and curing processes. It is believed that the drop in SE above 1000 MHz is due to the high-frequency leakage typical of a mesh material (having a high surface resistivity), which would also depend on the details of the composite structure for cured samples.

The electrical properties of an MGF-reinforced composite sample depend on the layup and curing process, which could be optimized for SE performance. Closer contact, longer fiber lengths, higher conductivity or thicker metallized layers, or higher MGF loading densities could improve the resulting composite material's σ_{eff} and hence the EM reflection. Future experiments will provide more definitive results for the applications of MGF in advanced shielding materials. These experiments include measuring the broadband SE of RoMHOglas™ cured in various ways to form planar and cylindrical samples. The layup and curing processes that produce the highest σ_{eff} will be identified and used to construct enclosure-size structures. Other shielding issues, such as the best way to form seams, embed metallic layers, or treat penetrations, can then be addressed.

References

1. R. H. Warfel, *Optimum Performance of Metallized Glass Fiber-Filled Composites*, 35th Annual Technical Conference, Society of the Plastics Industry (1980), Sec. 19-E, pp 1–6.

2. D. M. Bigg, *Mechanical, Thermal, and Electrical Properties of Metal Fiber-Filled Polymer Composites*, Society of Plastic Engineers, Inc., 37th Annual Technical Conference (May 1979), p 583.

3. Ronald J. Chase, *Composite Shielding Initiative for Army Resources*, U.S. Army Research Laboratory, ARL-SR-9 (June 1994).

4. John Latess, Calvin Le, and Joe Jaucian, *Investigations on the Use of Near Field Measurements to Determine the Effective Conductivity of Advanced Composite Materials*, U.S. Army Research Laboratory, ARL-TR-707 (July 1995).

5. Andrew A. Cuneo, Jr., and James J. Loftus, *Scale Modeling for the Perimeter Acquisition Radar EMP Test*, Harry Diamond Laboratories, HDL-TR-1761 (September 1976).

6. Andrew A. Cuneo, Jr., James J. Loftus, and Robert A. Dyckson, *EMP Scale-Model Testing of an Army Brigade Signal Center*, Harry Diamond Laboratories, HDL-TM-77-29 (December 1977).

7. Andrew A. Cuneo, Jr., and James J. Loftus, *Measurement of Scaled-Down HEMP Waveforms*, Harry Diamond Laboratories, HDL-TM-81-6 (March 1981).

8. Andrew A. Cuneo, Jr., and James J. Loftus, *Scale Modeling for the PATRIOT Electromagnetic Pulse Test*, Harry Diamond Laboratories, HDL-TM-81-16 (May 1981).

9. James J. Loftus, Valerie Fronczak, and Ira Kohlberg, *A Comparison of the Diffracted Fields as Measured and Predicted for a Totally Reflecting Fence in a Scale Model Test for an EMP Simulator*, Harry Diamond Laboratories, HDL-TR-2173 (February 1990).

10. W. L. Stutzman and G. A. Thiele, *Antenna Theory and Design*, John Wiley & Sons, Inc., New York (1981).

11. A. Papoulis, *The Fourier Integral and Its Applications*, McGraw-Hill Book Company, Inc., New York (1962).

12. D.R.J. White, *A Handbook on Electromagnetic Shielding Materials and Performance*, Don White Consultants, Inc., Germantown, MD (1975).

13. W. L. Gans, *Dynamic Calibration of Waveform Recorders and Oscilloscopes Using Pulse Standards*, IEEE Trans. Instrum. Meas. **39**, No. 6 (December 1990), 952–957.

14. A. M. Shaarawi and S. M. Riad, *Spectrum Amplitude of Step-Like Waveforms Using the Complete-FFT Technique*, IEEE Trans. Instrum. Meas. **34**, No. 4 (December 1985), 537–540.

15. S. M. Riad and R. B. Stafford, *Impulse Response Evaluation Using Frequency Domain Optimal Compensation Deconvolution*, IEEE Trans. Instrum. Meas. **34**, No. 4 (December 1985), 521–525.

16. J. G. Fairneny, *Flexible EMI/RFI Shielding Materials, Test Methods and Theoretical Relations*, U.S. Army Natick Research, Development and Engineering Center, NATICK/TR-95/007L (November 1994).

Distribution

Admnstr
Defns Techl Info Ctr
Attn DTIC-DDA (2 copies)
Cameron Sta Bldg 5
Alexandria VA 22304-6145

Director
Defns Intllgnc Agcy
Attn RTS-2A Techl Lib
Washington DC 20301

Defns Nuc Agcy
Attn RAES Elect Syst Techlgy Div
Attn RAST Electromagnetic Applctn Div
Attn TITL Tech Lib
6801 Telegraph Rd
Alexandria VA 22310-3398

Defs Nuc Agency
Office of Techl Applications
Attn D R Lewis
Alexandria VA 22310

HQ Dept of the Army
Attn DAMO-FDQ MAJ McGonagle
400 Army Pentagon
Washington DC 20310-0460

Cmdr
US Army ARDEC
Attn AMSTA-AR-AEC-IE N Svendsen
Picatinny Arsenal NJ 07806-5000

US Army ARDEC
Attn AMSTA-AR-AEF-A Chf
Adelphi MD 20783-1197

US Army AVRDEC
Attn AMSAT-R-EFM P Haselbauer
4300 Goodfellow Blvd
ST Louis MO 63120-1798

US Army BRDEC
Attn SATB-FGE J Ferrick
Attn SATB-FGE T Childers
FT Belvoir VA 22060-5606

Commander
US Army Matl Cmnd
Attn AMCAM-CN
5001 Eisenhower Ave
Alexandria VA 22333-0001

Director
US Army Mis Cmnd (USAMICOM)
Attn AMSMI-RD-CS-R Documents
Redstone Arsenal AL 35898-5400

Cmdr
US Army MRDEC
Attn AMSMI-RD-ST-CM J Vandier
Huntsville AL 35898-5240

US Army Natick RDEC
Attn SATNC-SUSD-SHD A Murphy
Kansas Stret
Natick MA 01760-5018

Commander
US Army Nuc & Chem Agcy
Attn MONA-NU R Pfeffer
7150 Heller Loop Rd Ste 101
Springfield VA 22150

Cmdr
US Army TARDEC
Attn AMSTA-ZT G Baker
Warren MI 48397-5000

Commander
US Army TECOM
Attn STERT-TE-E J Knaur
Redstone Technical Test Center
Huntsville AL 35898-8052

US Army TECOM Techl Dir Ofc
Attn AMSTE-TC-D R Bell
Aberdeen Proving Ground MD 21005

Distribution

Commander
US Army White Sands Missile Range
Attn STEWS-NE J Meason
White Sands Missile Range NM 88002-5180

Nav Rsrch Lab
Attn Code 4820 Techl Info Div
4555 Overlook Ave SW
Washington DC 20375-5000

Commander
Nav Surfc Weapons Ctr
Attn Code E231 Techl Lib
Dahlgren VA 22448-5020

Natl Inst of Stand & Techlgy
Attn V Ulbrecht Rsrch Info Ctr
Rm E01 Bldg 101
Gaithersburg MD 20899

US Army Rsrch Lab
Attn AMSRL-WT-WB Chf
Attn AMSRL-WT-WC Chf
Attn AMSRL-WT-WD Chf
Attn AMSRL-SL-CS B Smith
Attn AMSRL-WT-PB Chf
Aberdeen Proving Ground MD 21005

US Army Rsrch Lab
Attn AMSRL-OP-SD-TA Mail & Records Mgmt
Attn AMSRL-OP-SD-TL Tech Library (3 copies)
Attn AMSRL-OP-SD-TP Tech Pub
Attn AMSRL-SE Chf
Attn AMSRL-WT-N Chf
Attn AMSRL-WT-NB Chf
Attn AMSRL-WT-ND C Le
Attn AMSRL-WT-ND Chf
Attn AMSRL-WT-ND W O Coburn (10 copies)
Attn AMSRL-WT-NE Chf
Attn AMSRL-WT-NF Chf
Attn AMSRL-WT-NG Chf
Attn AMSRL-WT-NH Chf
Attn AMSRL-WT-NJ Chf
Attn AMSRL-WT-N Sr Rsrch Scntst
Attn AMSRL-WT-ND J Latess
Adelphi MD 20783-1197